A STATISTICALLY DESIGNED KARST FEATURE SURVEY, AND FACTORS CONTROLLING KARST FEATURE DENSITY AND DISTRIBUTION

by

Lorena Roque Martinez, B.S.

A thesis submitted to the Graduate Council of
Texas State University in partial fulfillment
of the requirements for the degree of
Master of Science
with a Major in Aquatic Systems
December 2019

Committee Members:

Benjamin Schwartz, Chair

Jennifer Jensen

Todd Swannack

FAIR USE AND AUTHOR'S PERMISSION STATEMENT

Fair Use

Duplication Permission

ACKNOWLEDGEMENTS

I would first like to thank my thesis advisor, Dr. Benjamin Schwartz, for his invaluable insight, unwavering encouragement, and patience. Thank you to my thesis committee, Dr. Jennifer Jensen and Dr. Todd Swannack, for their contributions.

Endless thanks to Chris Thomas, Facilities Manager of the Freeman Center, and to the folks at the Freeman Center for not only access to the ranch, but for the crucial advice on how to best navigate and prepare for those unforgiving 4,200 acres. I am greatly indebted to my field assistants and great friends, Aubri Jensen, Dalila Loiacomo, Olivia Jimenez, Lisa Koetke, Will Coleman, Alexis Commiskey, and Jared Haney, who gave up their early summer mornings to look for holes in the ground with me all while getting pricked by cacti. I must also thank Dr. Butch Weckerly and Dr. Andrew MacLaren for talking statistics with me whenever I needed it.

I am grateful to Dr. Marcus Gary for his support and for helping me acquire the resources I needed for this project; in particular for connecting me with Chris Thibodaux, who supplied the Camp Bullis geospatial data, to whom I also owe many thanks.

Finally, special thanks go to my family and friends for the moral support and encouragement throughout these demanding two years.

TABLE OF CONTENTS

Page

LIST OF TABLES

Table **Page**

LIST OF FIGURES

Figure **Page**

ABSTRACT

Karst feature inventories provide essential information used to evaluate a site's degree of hydrogeologic connectivity to local and regional flow systems, as well as its environmental and ecological sensitivity. For developments proposed on the Edwards Aquifer recharge zone, TCEQ rules require a full-coverage karst feature inventory of karst features during a geological assessment. However, visual surveys may be subjective, depending on the experience of the person performing a survey.

Considering this, my research focused on whether it is possible to develop an independent method for identifying the most sensitive recharge areas for visual surveys, when time and resources are limited, as well as provide a means for assessing the accuracy of surveys. The question motivating this research is: can relationships be identified between predictor variables and karst feature density that allow estimation of density without physical surveys?

A partial, statistically-designed, karst feature survey of the 17 km^2 Freeman Center of Texas State University in San Marcos, Texas resulted in 60 documented karst features, including three sinkholes ground-truthed from a GIS-based sinkhole detection method. The survey design used for Freeman was then tested on Camp Bullis, near San Antonio, TX, an area with known karst feature density, revealing that random surveying does not yield representative karst feature density results, as karst features tend to cluster.

The entirety of Camp Bullis was analyzed for factors that influence karst feature density. An Ordinary Least Squares model determined that slope, distance to nearest

flowline, lithology, and apparent resistivity were significant predictors of karst feature density ($R= 0.30$; $p<0.01$). A Geographically Weighted Regression was also used to visualize the nonstationarity of predictor variables ($R= 0.81$). However, both models resulted in spatial autocorrelation of residuals, indicating model misspecification. Despite concluding that karst features density is difficult to model, these methods offered a more nuanced understanding of factors controlling the distribution of karst features and the significance of these factors on Camp Bullis.

I. INTRODUCTION

Karst inventories are used to assess and quantify the number and type of karst features distributed on a landscape. These geospatial data can be used in combination with existing hydrologic and geologic data to quantify the vulnerability of groundwater and karst-adapted species to changes in land use and land cover. These data can then be used by managers to better understand connections between local and regional flow systems, manage areas of environmental and/or ecological sensitivity, and for mitigating hazards. As development expands onto karst areas, associated hazards, impacts (Gutiérrez et al., 2014), and potential for groundwater contamination rapidly increase (Lindsey et al., 2010). Geographic Information Systems (GIS) have been used extensively for analyzing spatial patterns of karst features (i.e., sinkholes or dolines), for hazard mapping, and vulnerability modeling. Studies from some USA states, including Minnesota (Gao et al., 2005), West Virginia (Doctor and Doctor, 2012), Florida (Brinkmann et al., 2008), and Kentucky (Florea et al., 2002) have used GIS to create and maintain regional karst data, and to analyze the spatial and morphometric characteristics in an objective manner to standardize karst feature detection and prediction for hazard and natural resource protection.

In the state of Texas, USA, the karstic Edwards Aquifer is designated as a sole-source aquifer for approximately two million people living in the city of San Antonio. Regionally, many other smaller towns and cities also depend, in-part, on water from the aquifer. Despite the aquifer's importance, a regional scale database of karst features and their distribution does not exist for its recharge zone, which is where nearly all surficial karst features occur. These types of data and studies are challenging to obtain or perform

in Texas due to the lack of a centralized and formal karst feature geodatabase. Although the Texas Commission on Environmental Quality (TCEQ) requires a geological assessment prior to all land development on the recharge zone, and that all karst features found during the state mandated geological assessments must be reported with coordinates to the TCEQ, these data are not made available to the public in an accessible format. With state population and water use projected to increase by 73% and 17%, respectively, over the next 50 years (TWDB, 2017) a simplified procedure for determining or predicting karst feature densities would be a helpful tool for regional land and water management, and could mitigate hazards and impacts to the aquifer.

Hydrogeologic Setting of the Edwards Aquifer

The Edwards Aquifer has three connected but hydrogeologically distinct zones: the contributing zone, the recharge zone, and the confined zone (Figure 1). The contributing zone is the area where water collects and flows downgradient toward the recharge zone. Once on the recharge zone, water quickly enters the aquifer through karst features in sinking streams. Sinking streams contribute up to 85% of all recharge to the aquifer (Slade et al., 1986), with diffuse upland recharge comprising the remaining 15%. The recharge zone is defined as the area where the lower Cretaceous-aged Edwards Aquifer hydrostratigraphic units crop out at the surface. These units are heavily karstified, faulted, and fractured due to the now-inactive, Oligocene-aged Balcones Fault Zone (BFZ) (Sharp and Banner, 1997), which allows meteoric water to quickly infiltrate into the subsurface where dissolution of carbonate rock by carbonic acid enlarges the faults and fractures to produce cavities and zones of exceptionally high permeability

(Barker et al., 1994). The SW-NE structure of the BFZ also controls regional flow in the Edwards Aquifer, allowing water to flow along or parallel to these SW-NE trending faults (Hunt et al., 2015). Rapid recharge through conduits, faults, and fractures, and high subsurface connectivity of conduits, means groundwater is sensitive to contamination (Hauwert et al., 2004).

Lastly, the confined zone is marked by the presence of the Del Rio clay of the upper Cretaceous, which confines the underlying Edwards Aquifer hydrostratigraphic units. The Edwards Aquifer is hydrologically bound underneath by a semi-confining unit; the upper member of the Glen Rose limestone. Down-dip, the deep boundary of the confined zone is marked by a transition from fresh water to brackish and saline waters with >1,000 mg/L total dissolved solids (TDS) (Slade et al., 1986).

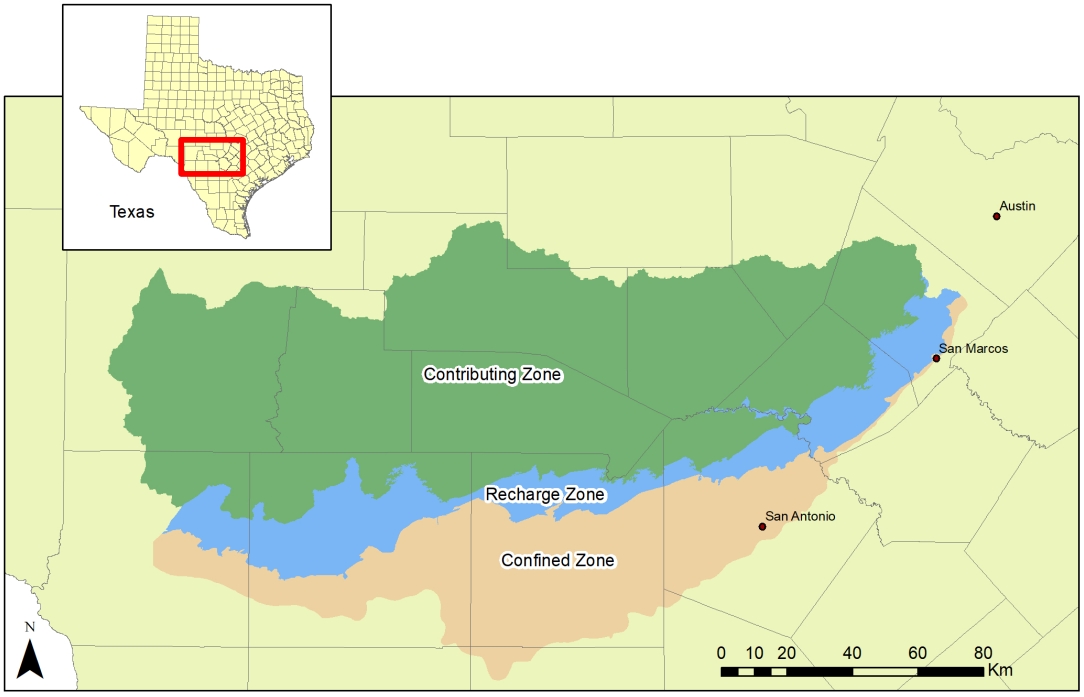

Figure 1. Edwards aquifer zones

Protection of the Edwards Aquifer Recharge Zone

Because several federally-listed as threatened or endangered species live in the aquifer or depend on groundwater discharge from large springs, they and their critical habitat, the Edwards Aquifer or related spring systems, are protected by the Endangered Species Act. Therefore, groundwater levels, spring flows, water quality, and groundwater extraction limits are maintained, enforced, and monitored by the Edwards Aquifer Authority (EAA, 2016). Because the recharge zone is the most sensitive portion of the aquifer system, the TCEQ requires licensed professional geologists to perform full-coverage geologic assessments before development and some other types of land disturbance in the recharge zone (TCEQ, 2008a) and contributing zone (TCEQ, 2008b). The main purpose of the surveys is to identify all features that may act as a connection between the surface and the aquifer, allowing for appropriate Best Management Practices (BMPs) to be applied, ensuring that the integrity of recharge features is maintained and impacts are lessened on existing features. Geological assessments include soil descriptions, geologic maps, stratigraphic columns, a general narrative of the site, and a geological assessment table, in which features are described based on their type and characteristics, and assigned a numerical score based on a list of parameters describing their sensitivity. A feature is considered "sensitive" and appropriate BMPs must be taken if a feature is assigned a score of >40. Features receive points for feature type, presence of lineaments or aligned features, and relative infiltration rates (TCEQ, 2004).

Although there are specific procedures and detailed descriptions and definitions for evaluating features, the nature of these surveys is subjective and depend on the experience of the surveyor. Geologists performing karst assessments may interpret and

classify karst features differently, depending on skill or experience. Because most of Texas is private land, access to land in the recharge zone is often limited or completely restricted prior to a development being planned and approved. In light of this, it would be it would be useful for planning and watershed/groundwater conservation and management purposes to have independent methods for estimating relative karst feature densities in different regions of the recharge zone.

Karst Feature and Sinkhole Distribution Analysis

Most distribution studies in karst areas focus on sinkhole distribution, as they present high potential for damage to infrastructure and public safety. In general, the typical explanatory variables used in these studies can be classified as hydrologic, structural, and anthropogenic. Selection of explanatory variables depends on knowledge of local controls for karstification, as well as data availability.

The typical starting point for any spatial analysis begins with Nearest Neighbor Analysis (NNA) which establishes whether any spatial pattern, clustered or dispersed, is present (Gao et al., 2005). For most sinkhole susceptibility studies, sinkhole density or distance to nearest sinkholes are used as the response variable (Doctor and Doctor, 2012). This requires establishing a scale to use as the search radius to calculate the response variables. Moreover, most pattern analysis toolsets on ArcGIS require user specification of a distance or bandwidth. Ripley's K function analyzes patterns of clustering/dispersion over a range of distances. Doctor et al. (2008) used this tool and its resulting peak clustering distance (1,200 m) to create their sinkhole density response variable. After this step, an Ordinary Least Squares (OLS) global linear regression model should be analyzed

for proper model specification (ESRI, 2019). Doctor and Doctor (2012) used OLS to check for collinearity in their explanatory variables. OLS is a global model and creates a single regression for the entirety of the study area. This assumes that the predictor variable relationships are constant throughout, which is unlikely in processes controlling formation of karst features, or sinkhole susceptibility, because the spatial pattern of variables controlling these processes are not uniform. As an answer to the issue of nonstationarity, the Geographically Weighted Regression (GWR) was created. GWR allows variable coefficients to vary through space by weighting them by their proximity to points being estimated (Fotheringham et al., 2002). Doctor et al. (2008) created a sinkhole susceptibility map for Frederick Valley, Maryland using GWR to model sinkhole susceptibility using the variables of proximity to quarries, water bodies, faults, fold axes, and groundwater table. Also using GWR, Doctor and Doctor (2012) used distance to fault, fold axes, fracture traces oriented along bedrock strike, fracture traces oriented across bedrock strike ponds, springs, quarries, depth to groundwater, and others to create a predicted sinkhole density map for Jefferson County, West Virginia. One crucial step to perform before running GWR is to choose an estimated bandwidth for the model. Of the options available in GWR, Doctor and Doctor (2012) determined that the best performing model used a fixed bandwidth established by the Ripley's K tool. That bandwidth was more conservative (1,750m, in their study) than the one used in creating their response variable to encompass the range of highest clustering and to avoid spatial dependence in the models.

Remote Sensing Methods for Sinkhole Detection

Relatively new remote sensing technologies and methods can be used to produce highly detailed topographic maps, or surface elevation data, which can be used to detect sinkholes using GIS. Light Detection and Ranging (LiDAR is an active remote sensing technique that measures range from time between laser light pulse emission and detection upon return (NOAA., 2012). A single light pulse can have several return detection times, creating what are called point clouds (NOAA, 2012). The high density of light pulses and multiple returns allow for penetration between gaps in dense vegetation canopy to the ground surface, allowing for karst feature studies in areas where imagery is insufficient to detect features on the surface (Kobal et al., 2014). Use of LiDAR has shown great success in detecting sinkholes in karst, and airborne LiDAR can produce large swaths of high accuracy and high-resolution data for regional scale projects. Its ability to penetrate gaps in vegetation canopy enables research that would otherwise have been impossible without time consuming and strenuous field work, and LiDAR data used in tandem with computer learning methods shows great promise in improving sinkhole-detection success rates (Zhu and Pierskalla, 2016).

Most karst detection methods using LiDAR begin by creating a digital terrain model (DTM) from LiDAR ground points (Panno and Luman, 2018). After DTM creation, there are a handful of options for detecting sinkholes. Of these, manual detection (Zhu et al., 2014), contour tree method (Wu et al., 2016), and sink filled-difference (Doctor and Young, 2013) are among the most popular. After potential sinkholes are extracted from the data, morphological parameters can be calculated and used to filter out depressions unlikely to be natural karst depressions (i.e., anthropogenic

features). Zhu and Pierskalla (2016) selected 11 parameters that helped detect true sinkholes: 3 surficial shape-based variables, 4 depth-based variables, 2 natural and human factors, and 2 variables that aided in field observations. Morphological parameters, such as a circular index or a conical shape, are common in most published studies.

Case Study: Camp Bullis and Geophysical Methods for Karst Detection

The Camp Bullis Training Site is military training facility in northern Bexar County. Most of the area is dominated by the Glen Rose Limestone, except for the southeastern corner where faulting has juxtaposed the younger Kainer Formation from the Edwards Group with the older Glen Rose units (Clark, 2003). The Glen Rose Limestone typically has lower permeability and porosity than the Edwards limestone but in this area, it is uncharacteristically permeable and porous (Veni, 1994).

A geodatabase of surveyed karst features allowed for creation of karst feature density zones (KFDZs) bounded by lithological contacts and faults. A raster of KFDZs was compared to results of a USGS helicopter electromagnetic survey at different depths and showed high correlation to the KFDZs (Gary et al., 2003).

Additionally, two caves in Camp Bullis were monitored for five years to study vadose recharge during dye traces, and natural and artificial recharge events. Effective recharge at KFDZs were calculated by spatially extrapolating the effective recharge at the two caves based on a typical rain event for Camp Bullis of 2.7 cm. Recharge rates for a typical rain event, with wet antecedent conditions, reached 8.6 L/m^2 for the largest cave.

The degree of detail and wealth of information garnered from this study could not have been possible without a robust karst feature geodatabase. In summary, it allowed for

correlation with EM surveys, delineation of karst feature densities, and estimation of effective recharge for the entire study area. This study highlights the need for a centralized GIS integrated geodatabase for karst features for the Edwards Aquifer because it illustrates the power of using mapped karst features to answer hard questions such as how much a study area's recharge features contribute to the local flow system. The Camp Bullis study is largely the motivation for this thesis.

Research Objective

Considering the time and effort required to perform a typical full-coverage geologic assessment and karst feature inventory, the objective of this study was to investigate potential relationships between karst feature density and hydrologic, geologic, and geomorphic factors by surveying an area within the Edwards Aquifer recharge zone. The research question addressed in this study is: **can karst feature density be predicted using geologic, spatial data, and a statistically designed incomplete karst feature inventory**? If so, this would allow managers to estimate relative vulnerability and karst feature densities across the recharge zone prior to (or perhaps instead of) a comprehensive on-the-ground survey.

II. METHODS

This study consisted of four parts: 1) a partial karst feature field survey of the Freeman Center, an area with unknown karst feature density in the recharge zone. The results of the survey were analyzed for relationships between karst feature density and possible predictor variables; 2) a sinkhole detection method using LiDAR-derived elevation data and GIS that was ground-truthed during the karst feature survey, 3) evaluation of the efficacy of a karst feature field survey design for the Freeman Center by testing it on existing full-coverage Camp Bullis karst feature data, and 4) exploring the spatial patterns of karst features within Camp Bullis. All geospatial methods used were performed using ArcGIS 10.5.

Study Area - Freeman Center

The Texas State University Freeman Center (Freeman Center) is an approximately 17km^2 (4,204-acre) experimental and working ranch that lies entirely within the recharge zone of the San Antonio segment of the Edwards Aquifer in Hays County, TX (Figure 2). The Freeman Center is nearly undeveloped except for a few administrative buildings and shelters for cattle and storage and is used almost entirely for grazing rangeland. Land cover consists primarily of dense thickets of Plateau Live Oak (*Quercus fusiformis*) and Ashe Juniper (*Juniperus ashei*), or open savanna composed of mixed grasses and trees. Geologically, the Center (Table 1) lies within the Hueco Springs Fault Block and on the San Marcos platform, and is in an area where members of the Edwards Limestone dominate the surficial geology (Johnson et al., 2012) and several mapped faults cross the study area (Figure 3).

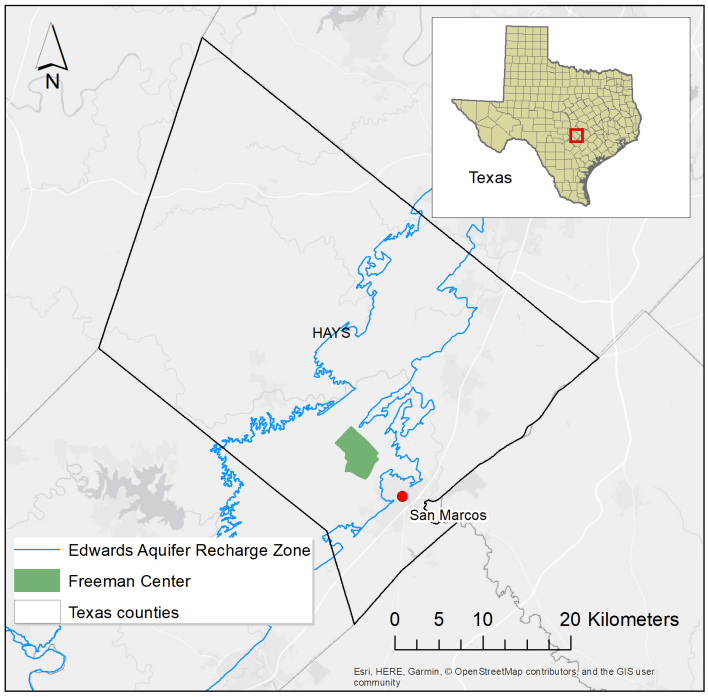

Figure 2. Freeman Center location

Table 1. Hydrostratigraphy of surficial geology on the Freeman Center

Age	Formation	Member	Hydrostratigraphy
Upper Cretaceous	Kb- Buda Limestone	undivided	Upper Confining Units
	Kdr- Del Rio Clay		
Lower Cretaceous	Kg- Georgetown Formation	undivided	Edwards Aquifer
	Person Formation	Kpcm- Cyclic and Marine	
		Kpcl- Leached and Collapsed	
		Kprd- Regional Dense	
	Kainer Formation	Kkg- Grainstone	
		Kkke- Kirschberb evaporite	
		Kkd- Dolomitic	

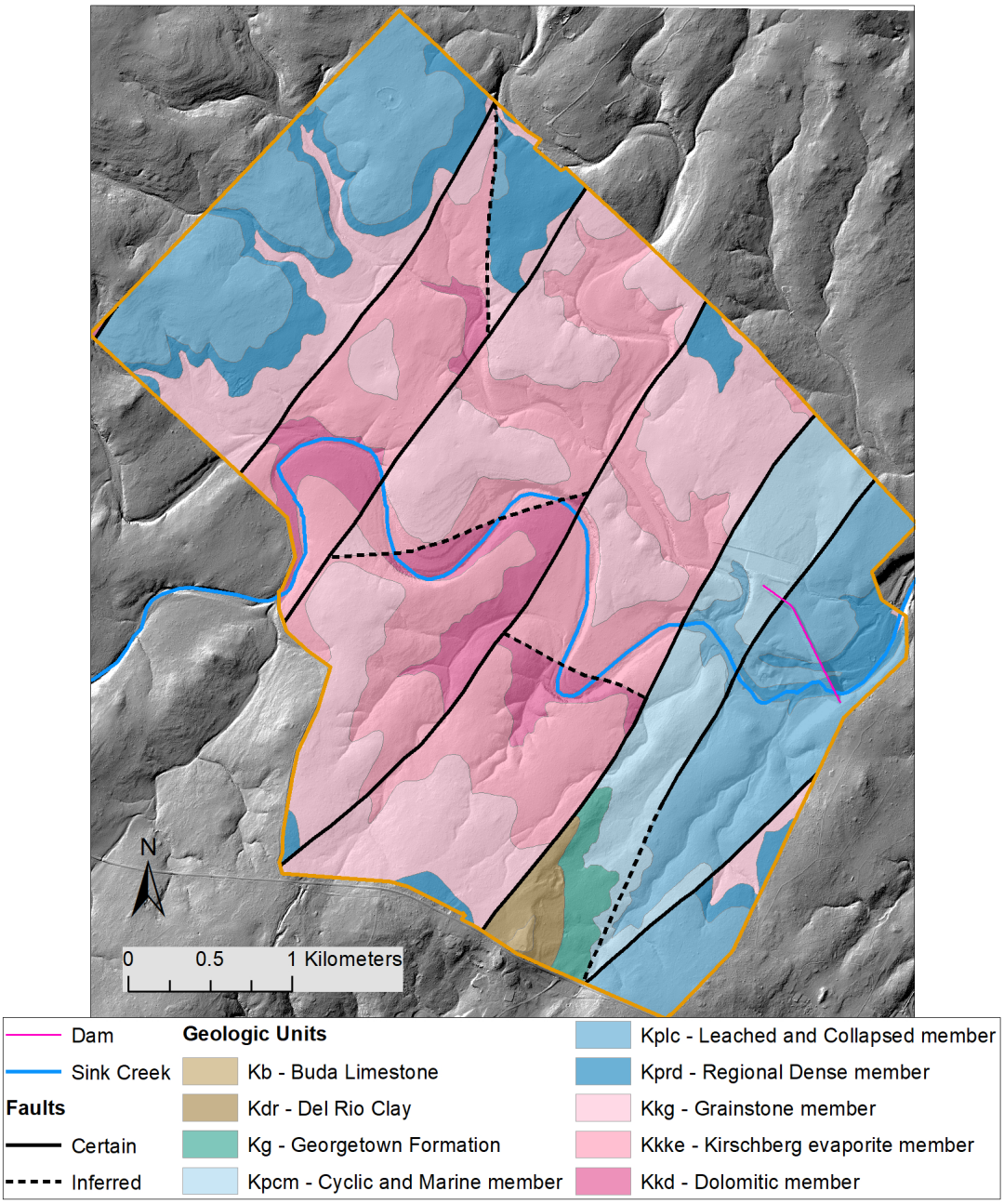

Figure 3**.** Geologic map of the Freeman Center. Note that Sink Creek is normally dry and only flows briefly after very large flooding precipitation events.

Freeman Center- Karst Feature Detection

LiDAR data used for this analysis were retrieved from Capital Area Council of Governments (CAPCOG, 2012), and was acquired during a 2008 survey during leaf-off

conditions; optimal for creation of a bare earth DTM. The LAS-to-raster tool in ArcGIS was used to create a DTM of Freeman using only ground-return LiDAR points, using average cell assignment and a natural neighbor interpolation method. Hillshade and slopeshade rasters were then derived from the DTM for enhanced visualization of topographical features. These rasters, along with the orthoimagery from Texas Natural Resources Information System (TNRIS, 2015) were used to manually delineate and digitize potential depressions through close visual inspection (Figure 4). Orthoimagery is helpful in deciphering whether depressions detected in the DTM are natural or anthropogenic. Greyscale and green to red gradient slopeshade rasters help define boundaries of depressions. Although manual delineation using high resolution DTMs is a step up from traditional, topographic map methods, it is time consuming and somewhat subjective. Automated methods have the ability to capture all depressions in a more complete way (Wall et al., 2017), within the limitations of data resolution.

Extracting sinkholes from LiDAR in ArcGIS was relatively simple (Figure 5) and followed the sink filled-difference method of Doctor and Young (2013). All operations for ArcGIS HydroTools work under the assumption that water flows downslope in the direction of least resistance (i.e., steepest gradient). However, it is typical to find 'sinks' in a DTM. Sinks are cells that are surrounded by other cells of higher elevation, thus impeding downgradient flow. The Fill tool was originally created to correct what are often simply small errors in elevation, by raising the elevation of all cells in a sink to allow flow to continue downgradient to other cells, for the purpose of watershed delineation (Maidment, 2002). However, in karst terrain, it is possible for sinks to be real depressions or sinkholes and not elevation errors in the DTM. The Fill tool creates a new

raster with filled sinks and 'corrected' elevations that allow flow downgradient. Before use of the Fill tool one must also consider the presence of artificial dams like bridges over streams and ditches/excavations, or, in the case of the Freeman Center, a large flood-control dam that create false sinks. Without reconditioning the DTM to allow streams to drain through the dam on Sink Creek at Freeman, the sink raster results in a false sink (Figure 6). Doctor and Young (2013) recommend 'burning the stream channels' (i.e., hydroenforcement) through these features by manually digitizing the stream channels and lowering the elevation along them using the DEM Reconditioning tool in ArcGIS.

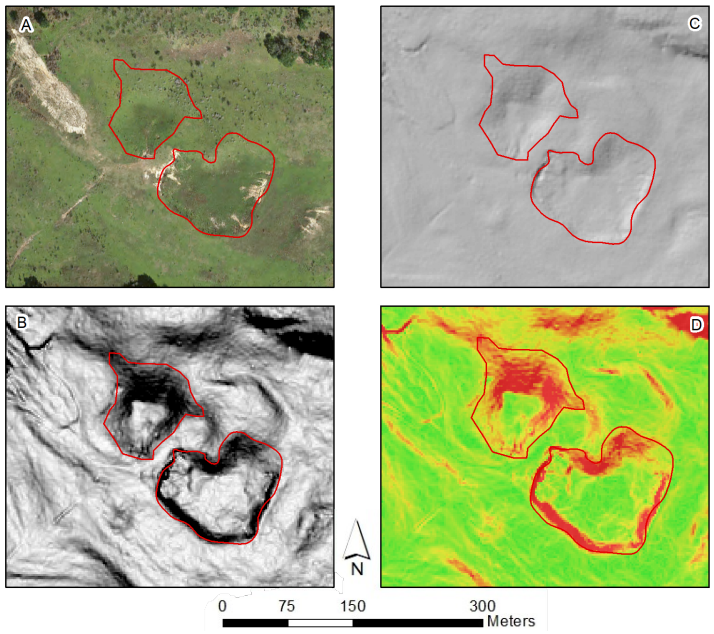

Figure 4. Example of manual delineation of depressions. Depressions outlined in red required toggling between several images: A) orthoimagery, B) greyscale slopeshade with darker colors symbolizing steep slope, C) hillshade, and D) green to red gradient slopeshade with red symbolizing steep slope

After reconditioning, the Fill tool was used to identify sinks in the DTM, and the new filled raster was subtracted from the original DTM using the Raster Algebra tool to create a sink raster. Consequently, cells in the sink raster are attributed with elevation

differences between the original DTM and the reconditioned DTM and represent sink depth. This raster was then reclassified to show values below a vertical depth threshold of (0.37m) as 'NoData'. This step filtered out what were most likely errors in the LiDAR and too shallow to be of any hydrological significance. This threshold should be a value larger than or equal to the vertical residual mean square error (RMSEz) of the LiDAR data used to create it. The RMSEz of this LiDAR in non-vegetated areas is 0.185 meters. Finally, the raster to polygon tool was used to change the raster cells with values to polygon features.

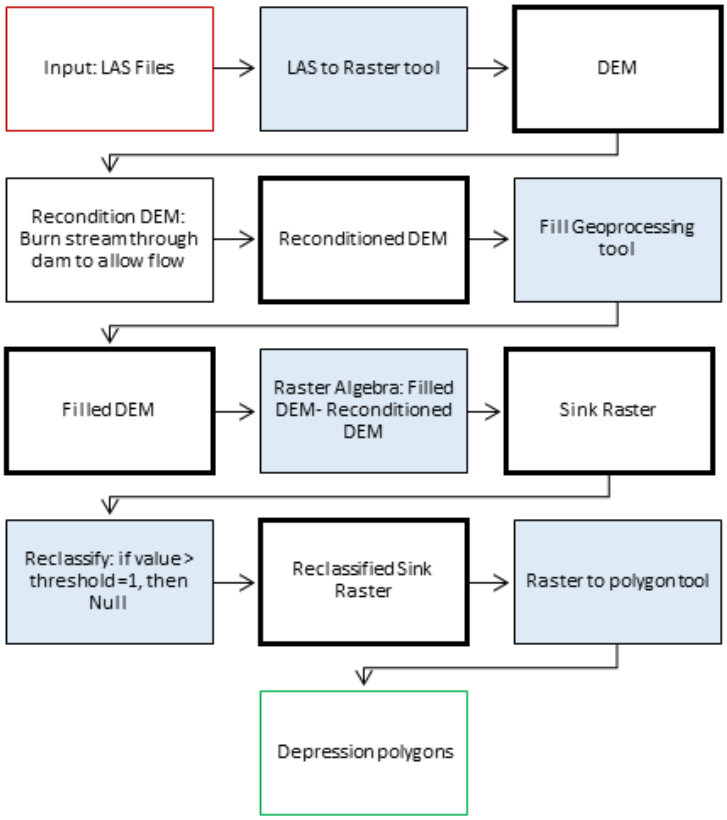

Figure 5**.** Workflow for extracting depressions from LiDAR data. Bold steps indicate outputs and blue steps indicate tools.

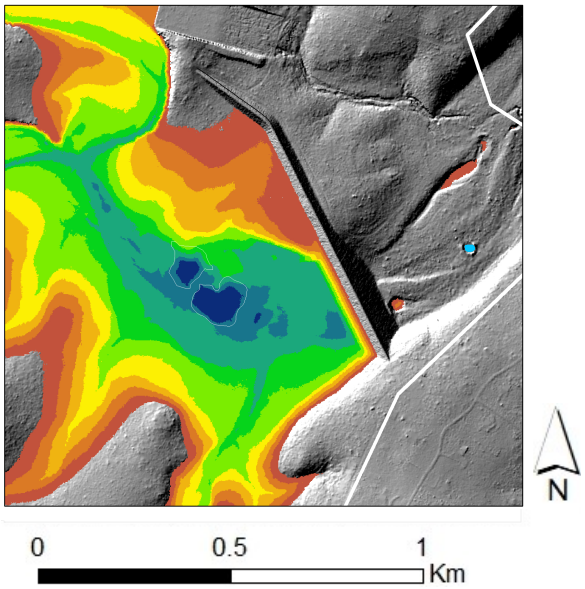

Figure 6**.** Dam impeding flow resulting in a false sink. The channel elevation must be lowered (burned) through the dam to allow for drainage and true sinks to be identified. Also visible are some of the many natural scour features in the dry Sink Creek channel that are detected as 'sinks'

Freeman Center Karst Feature Field Survey

A partial-coverage survey of the Freeman Center was performed. To ensure proportional surveying of each geological unit found on the Freeman Center, 202 30m x 30m survey plots were randomly distributed in proportion to the surface area of each geological unit exposed. Of the nine geological units exposed on the Freeman Center, three combined cover less than 5% of the study area (Buda, Del Rio, and Georgetown) and were therefore pooled for statistical reasons. Pilot tests determined that surveying a 30 m x 30 m ($900m^2$) plot required approximately 40 minutes, and that ~200 plots could be surveyed in three to four months during the summer. Plot locations were determined by randomly generating points in ArcGIS using the number of points presented in Table 2.

Teams of two people performed field surveys. After locating the survey point with GPS, plot boundaries were measured and defined, and surveyors completed a full-

coverage survey in the 900m^2 plot for karst features. Five soil depth measurements per plot (one at each corner and the center) were obtained by hammering rebar into the ground until refusal.

For each karst feature identified, its location and attributes were documented in the field using the Esri Collector application (Esri, 2017). Collector allows surveyors access to a downloaded map with editable layers like karst feature points, lines and polygons, and non-editable layers such as survey points, fences, gates, soils, geology, hillshade, slopeshade, and 2015 orthoimagery available from Texas Natural Resources Information System (TNRIS) at 50cm resolution. Collector was used as a tool for both navigation and data collection. After each day of fieldwork, edits were synced to the original map in ArcOnline. After field surveying was complete, the resulting edited point and line karst feature files were exported to ArcMap and saved.

Table 2. Survey plots in each geologic unit

Unit Abbreviation	Unit Name	Percent of Total Area	Calculated Plots	Final Plots
Kb Kdr Kg	Buda Limestone Del Rio Clay Georgetown	2.77%	5.542	6
Kkd	Dolomitic	6.34%	12.675	13
Kkg	Grainstone	27.44%	54.886	55
Kkke	Kirschberg	26.26%	52.528	53
Kpcm	Cyclic and Marine	7.86%	15.725	16
Kplc	Leached and Collapsed	20.95%	41.899	42
Kprd	Regional Dense	8.37%	16.747	17
	TOTALS	100%	200.002	202

Freeman Center - Potential Predictor Variables for Karst Feature Density

Variables tested for correlation with karst feature density were surface geology, slope, soil depth, soil type, distance to nearest fault, and distance to nearest flowline. All geological and structural data were accessed from the USGS (Blome et al., 2005). Geologic units are defined by differences in rock composition and presence or absence of fossils; some of which may be more conducive to dissolution and creation of karst features. For example, due to its high evaporite content (nodular gypsum), the Kirschberg evaporite member of the Edwards group that encompasses 26% of Freeman is known in other areas to have extensive karst feature development (Stein and Ozuna, 1994). Slopes can affect karst density if they are steep enough to expose enlarged bedding planes and, because steeper slopes also cause higher soil erosion, these areas can expose enlarged bedrock fractures or fissures. Karst feature density can be affected by soil depth simply because thick soils can cover or fill features that might otherwise manifest on the surface in areas with thinner or no soil cover. Two soil types dominate the Freeman Center; the Comfort-Rock and Rumple-Comfort soils cover approximately 97% of the Center combined (Figure 7). These soils are usually 33-91 cm thick, lie directly on the bedrock, and are well-drained residuum weathered from limestone (USDA Soil Conservation Service, 1984). Karst density can also be affected by distance to faults due to the tendency of faults to control regional and local flow routes in the Edwards Aquifer by providing fracture zones where preferential flow and dissolution may occur.

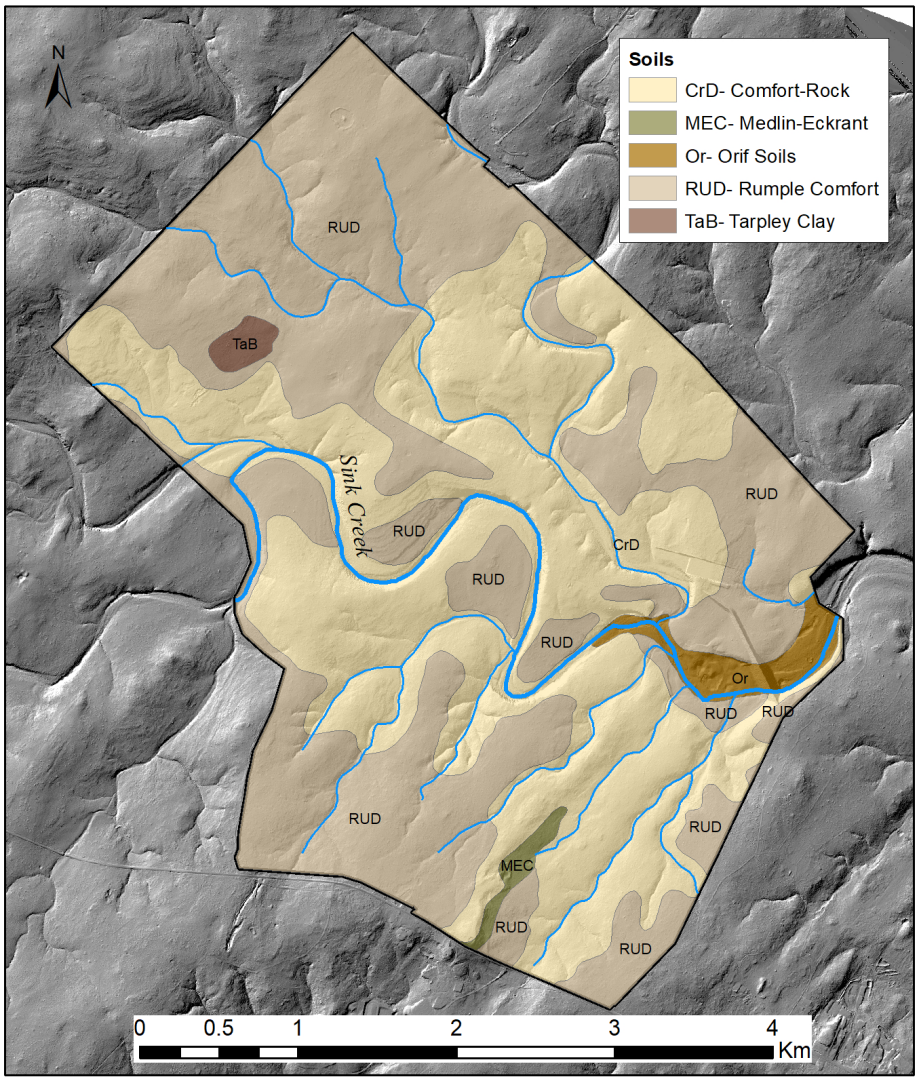

Figure 7**.** Soil map of the Freeman Center (USDA, 2017)

Freeman Center- Statistical Analysis

After completion of the survey, each plot was attributed with a karst feature density (# of features/area), karst feature count, average slope (degrees), dominant soil type, surface geology, average soil depth, and Euclidean distance to nearest fault and to nearest flowline. Slope and flowline data were derived from the LiDAR-derived DTM.

Because the response variable (karst feature count) is non-normal and 78% are zeros, the glmmTMB package of RStudio (RStudio, 2017) was used to run a zero-inflated fully saturated Poisson model to identify significant predictors. The model statement is below:

$$\text{Karst feature count} = \beta_0 + \beta_1 * \text{soil depth} + \beta_2 * \text{slope} + \beta_3 * \text{proximity to fault} + \beta_4 * \text{proximity to flowline} + \beta_5 * \text{geology type} + \beta_6 * \text{soil type} + \varepsilon$$

Testing Efficacy of Freeman Survey Design

A full-coverage karst feature survey data of Camp Bullis was used in this study to test the efficacy of the karst feature survey design utilized on the Freeman Center. Camp Bullis is a 113 km^2 military training facility, 65 km southwest of the Freeman Center, in Bexar County near the city of San Antonio, Texas. Unlike the Freeman Center, which is completely within the Edwards recharge zone, only the southeastern corner of Camp Bullis is in the recharge zone where the Kirschberg evaporite and dolomitic members of the Edwards units crop out (Clark et al., 2016). To make direct comparisons between the two sites, only the geologically equivalent areas of Camp Bullis were used to test our survey design. A similar proportionate amount of 30 m x 30 m plots (103) were randomly distributed within the two geologic units Bullis has in common with Freeman. Each plot would then capture known karst feature locations and karst feature density (karst features/area) could be calculated.

Camp Bullis Karst Feature Distribution

As opposed to only using the Edwards units in the southeastern corner for testing Freeman survey efficacy, the following methods were used to study feature distribution within the entirety of the Camp Bullis study area. The Average Nearest Neighbor tool on ArcGIS was used to determine if any spatial patterns to karst features exist. The NNA corroborates what is readily visible from the karst feature map of Camp Bullis (Figure 8), which is that karst features on Camp Bullis are clustered ($p < 0.01$), with a nearest neighbor ratio (observed mean distance/expected mean distance) of 0.46.

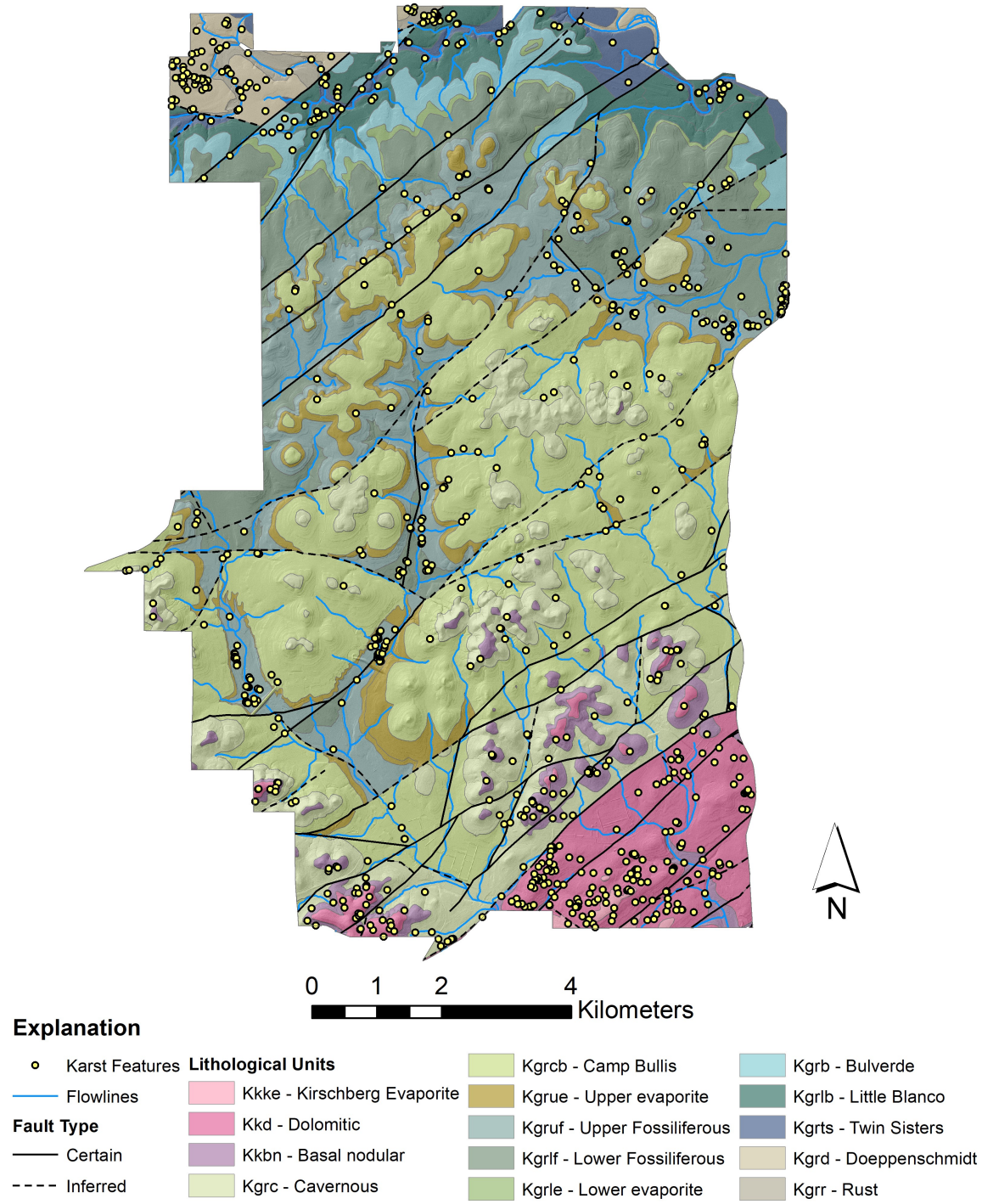

Figure 8. Karst features within Camp Bullis

The next step was to create the response variable of Karst Feature kernel density. To run the kernel density tool, a search radius needs to be established. To determine the

appropriate radius for clustering and therefore the scale at which factors controlling karst feature clustering are operating, the Multi-Distance Spatial Cluster (Ripley's K Function) in ArcGIS was used. Inputs were the Camp Bullis karst feature points feature class with the following specifications: starting distance (10 m), distance increment (40 m), number of distance bands (100), study area (Camp Bullis boundary polygon feature class), edge correction method (simulate outer boundary). If no study area is selected, a minimum-enclosing rectangle is generated by the tool and is used as the study area polygon. I opted against the minimum enclosing rectangle because it would have included areas that were not searched and surveyed and could lead to erroneous edge estimates. Another edge correction available is the Ripley's edge correction formula. This method gives extra weighting to neighbors whose distance from the point of interest is greater than their distance from the edge. This method however is only appropriate for a minimum enclosing rectangle study area and therefore inappropriate when using the actual study area.

Results from the Ripley's K indicate that clustering increases until it reaches peak clustering at 1,010 m (Figure 9). The kernel density tool was used to calculate karst feature kernel density (KFKD, the response variable) (features/ km^2) for each karst feature location using the peak clustering distance, independently determined by Ripley's K as 1,010 m, as the search radius (Figure 10).

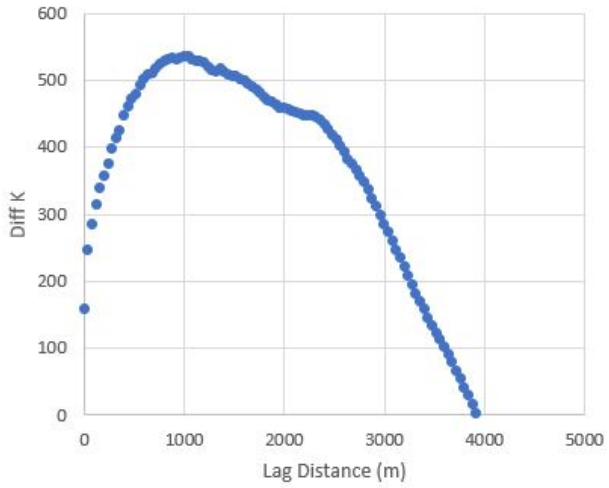

Figure 9. Ripley's K results. This graph indicates clustering vs lag distance. Diff K is equal to Observed K values – Expected K values. Clustering peaks at 1,010 meters and then decreases.

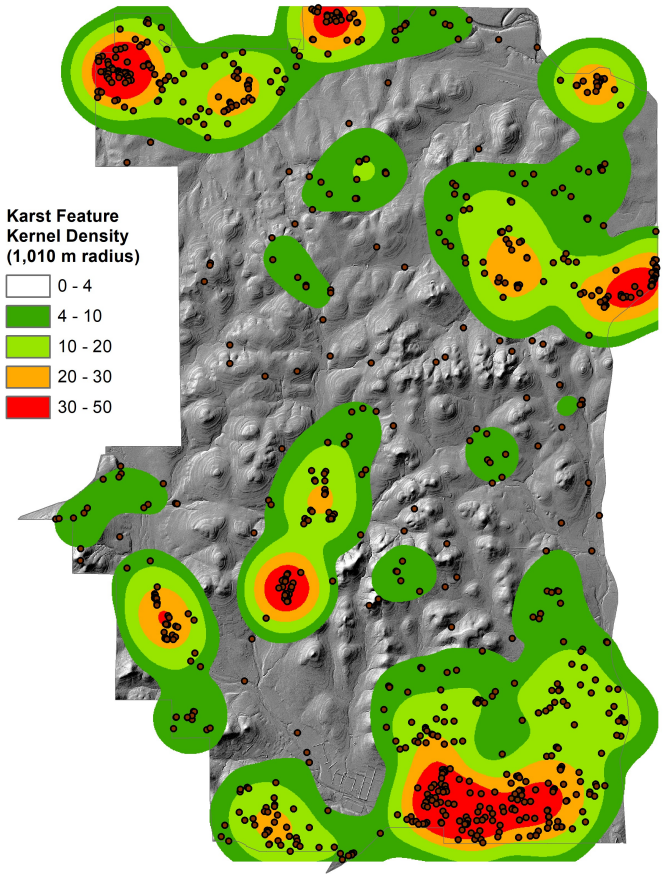

Figure 10. Camp Bullis KFKD map (features/km^2). Points indicate karst features.

Ordinary Least Squares Regression

KFKD was used as the response variable in the Ordinary Least Squares regression tool in ArcGIS to evaluate explanatory variable significance and proper model specification. Explanatory variables used were: Euclidean distances to nearest flowline (TNRIS, 2014) and fault, slope in degrees, and apparent resistivity (Ohm-meters). The model statement is below:

$$KFKD = \beta_0 + \beta_1 * \text{resistivity} + \beta_2 * \text{slope} + \beta_3 * \text{proximity to fault} + \beta_4 * \text{proximity to flowline} + \varepsilon$$

To quantify apparent resistivity, and in an effort to have a continuous variable that could distinguish different hydrogeological units, I chose to visually determine apparent resistivity from data presented in Smith et al. (2015) who concluded that the highest frequency of 115 KHz produces apparent resistivity that is most closely correlated with hydrogeological units. The OLS regression in ArcGIS also calculates diagnostics that help determine model performance. The model returns a Variance Inflation Factor (VIF) for each predictor where a VIF of 7.5 or higher indicates redundancy. The Koenker statistic evaluates the stationarity of the model where the null hypothesis is that the model exhibits stationarity and therefore that the relationships modeled are consistent across space. The Jarque-Bera (JB) statistic evaluates the normality of residuals where the null hypothesis is that the residuals are normally distributed.

Geographically Weighted Regression

A GWR was used as a tool to visualize the non-stationarity of variable relationships. The explanatory variables used to estimate KFKD in the GWR were the

same as those used in the OLS regression: euclidean distances to nearest flowline and fault, slope, and apparent resistivity. Following methods in Doctor and Doctor (2012), I chose a more conservative fixed bandwidth of 1,370 m to run the GWR. This encompasses a wider range of the highest clustering and avoids introducing dependence into the model, as it differs from the bandwidth used to calculate KFKD. The model statement below:

$$KFKD = \beta_0 + \beta_1 * \text{resistivity} + \beta_2 * \text{slope} + \beta_3 * \text{proximity to fault} + \beta_4 * \text{proximity to flowline} + \varepsilon$$

III. RESULTS

Sinkhole Detection on the Freeman Center

The LiDAR-based sinkhole detection method identified 414 'sinks' deeper than 0.37 m with an area greater than 16m^2 (4 times the cell size). Of these, 81% are within 10 meters of a flowline (Figure 11) and are likely false positives that reflect the chaotic stream bed morphology. In the field, this topography was confirmed and is composed of storm debris like large downed trees and boulders, as well as scours and other erosional features. This however does not indicate an absence of karst features, as sinking streams contribute up to 85% of all recharge to the Edwards Aquifer (Slade et al., 1986). As an example of how important small in-stream features can be, at least one 8.5 m deep cover-collapse sinkhole exists in the Sink Creek channel, and this feature alone has the capacity to recharge most of the surface flows in Sink Creek that occur on the Freeman Center (pers com – Freeman Ranch Manager). Despite the large number of false positives across the study area, three true positive subsidence sinkholes greater than 30 meters in diameter were field verified; all of which were previously unknown to Center management.

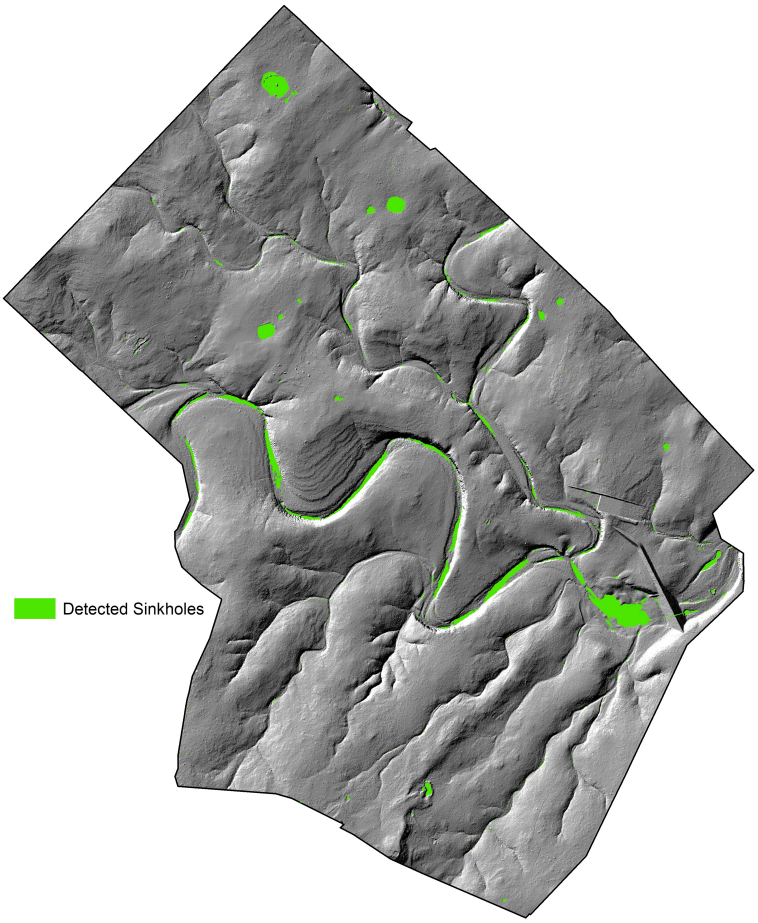

Figure 11. Sinkholes detected at the Freeman Center. These sinkholes have a depth greater than 0.37m and area larger than 16m^2. Note that most features along drainage channels are not actual sinkholes and are the result of erosion and deposition in the channel.

Freeman Karst Feature Survey

Of the 202 plots surveyed, 45 had karst features. Of the 60 karst features found within those plots, 34% are subsidence sinkholes, 30% solution cavities, 18% solution enlarged fractures, and 3% faults (Table 3). Plots contained 0-3 features. The zero inflated fully saturated Poisson model identified slope as the only significant predictor ($p < 0.05$) of karst feature counts in the plots (Table 4). Therefore, surface geology, soil type, distance to nearest fault and flowline, and soil thickness were not significant in explaining the variation in karst feature count in this model.

Table 3. Freeman karst feature survey results within plots

Feature Type	**Count**	**Percent**
sinkhole (subsidence)	24	34%
solution cavity	21	30%
solution-enlarged fracture	13	18%
fault	2	3%
TOTAL	60	100%

Table 4. Poisson model output

Variable	**Estimate**	**Standard Error**	**p-value**
Intercept	-1.970 e+01	7.469e+03	0.998
Kkd	1.768 e+01	7.469e+03	0.998
Kkg	1.805 e+01	7.469e+03	0.998
Kkke	1.804 e+01	7.469e+03	0.998
Kpcm	1.862 e+01	7.469e+03	0.998
Kplc	1.799 e+01	7.469e+03	0.998
Kprd	1.891e+01	7.469e+03	0.998
Soil- Rumple Comfort	-6.232e-02	3.344e-01	0.852
Proximity to stream	7.570e-04	2.621e-03	0.773
Proximity to fault	7.659e-04	9.620e-04	0.426
Average soil depth	9.430e-03	5.381e-02	0.861
Average slope	1.534e-01	7.792e-02	0.049

An additional 34 features were documented outside of the plots while walking along the terrain. 11 non-karst features like burrows were also documented within the plots. Neither were used for this analysis. The total amount of features recorded was 105.

Testing Freeman Survey Efficacy

Freeman results are valid under the assumption that the plots sampled are representative of the actual karst feature density in the study area. This assumption was tested by applying the same sampling methods to an area with full a coverage karst feature survey and a resulting known karst feature density; Camp Bullis. A proportionate number of plots (103) were randomly distributed in Camp Bullis within the two lithological units it has in common with the Freeman Center. Of those 103 plots, just one plot captured two features, resulting in a karst feature density of 21.57 karst features/km^2 for the dolomitic member of the Kainer formation (Kkd). Based on data from the full-coverage karst feature survey of Camp Bullis, the true density is 27.65 karst features/km^2. Although the survey design appears to result in similar karst feature densities, the results are more than likely random chance given that only one of the randomized plots captured two features. Randomizing survey plots in an area where karst features are clustered will result in underestimating karst feature density if survey plots miss clusters, or overestimating karst feature density if they capture clusters of karst features.

Camp Bullis Karst Feature Distribution - Ordinary Least Squares

Results of the OLS analysis of the full Camp Bullis dataset indicate that all predictors are significant (Table 5). The OLS tool on ArcGIS computes standard error, t-statistic, and probabilities that are robust against non-stationarity. Table 6 presents results for diagnostics calculated for the model.

Table 5. OLS regression coefficients

Variable	Coefficient	Robust Standard Error	Robust Probability	VIF
Intercept	16.519951	1.008121	$p < 0.0001$	-------
Slope	-0.354402	0.048447	$p < 0.0001$	1.019060
Flowlines	-0.015897	0.002260	$p < 0.0001$	1.080969
Faults	0.005090	0.001495	$p < 0.0001$	1.012003
Resistivity	0.050770	0.002720	$p < 0.0001$	1.06793

Table 6. OLS diagnostics

Diagnostic	Value	Probability
Adjusted R^2	0.303355	-------
Joint Wald Statistic	465.631768	$p < 0.0001$
Koenker Statistic	61.200504	$p < 0.0001$
Jarque-Bera Statistic	48.328784	$p < 0.0001$

The VIF for all explanatory variables were below the critical value, indicating that multicollinearity is not an issue. The Koenker statistic was statistically significant, which indicates non-stationarity. This test indicates that the GWR model is appropriate, which accounts for the non-stationary nature of these relationships by allowing coefficient estimates to vary. The Jarque Bera was statistically significant and indicates that the model is biased, i.e., the model is missing an explanatory variable. A Spatial Autocorrelation (Moran's I) test on the residuals revealed spatial autocorrelation with a Moran's I Index of 0.60.

Despite the obvious model misspecification, I ran a GWR model for Camp Bullis as an exploratory investigation into the spatial variability of the predictors.

Camp Bullis - Geographic Weighted Regression

The overall adjusted R^2 for the GWR is 0.81, compared to the global OLS adjusted R^2 of 0.30. I ran a Spatial Autocorrelation (Moran's I) on the residuals with a fixed distance band of the peak clustering distance (1,010 m) and it again determined clustering of residuals ($p < 0.01$) with a Moran's Index of 0.15. To investigate sensitivity to scale I re-ran the Spatial Autocorrelation tool at a bandwidth of 1,370m, the same used in the GWR, and it also determined clustering of residuals ($p<0.01$) with a Moran's Index of 0.06. Figure 12 shows local R^2 values indicating better model performance with warming colors. Figure 13 shows explanatory variable coefficient value rasters with local R^2 points.

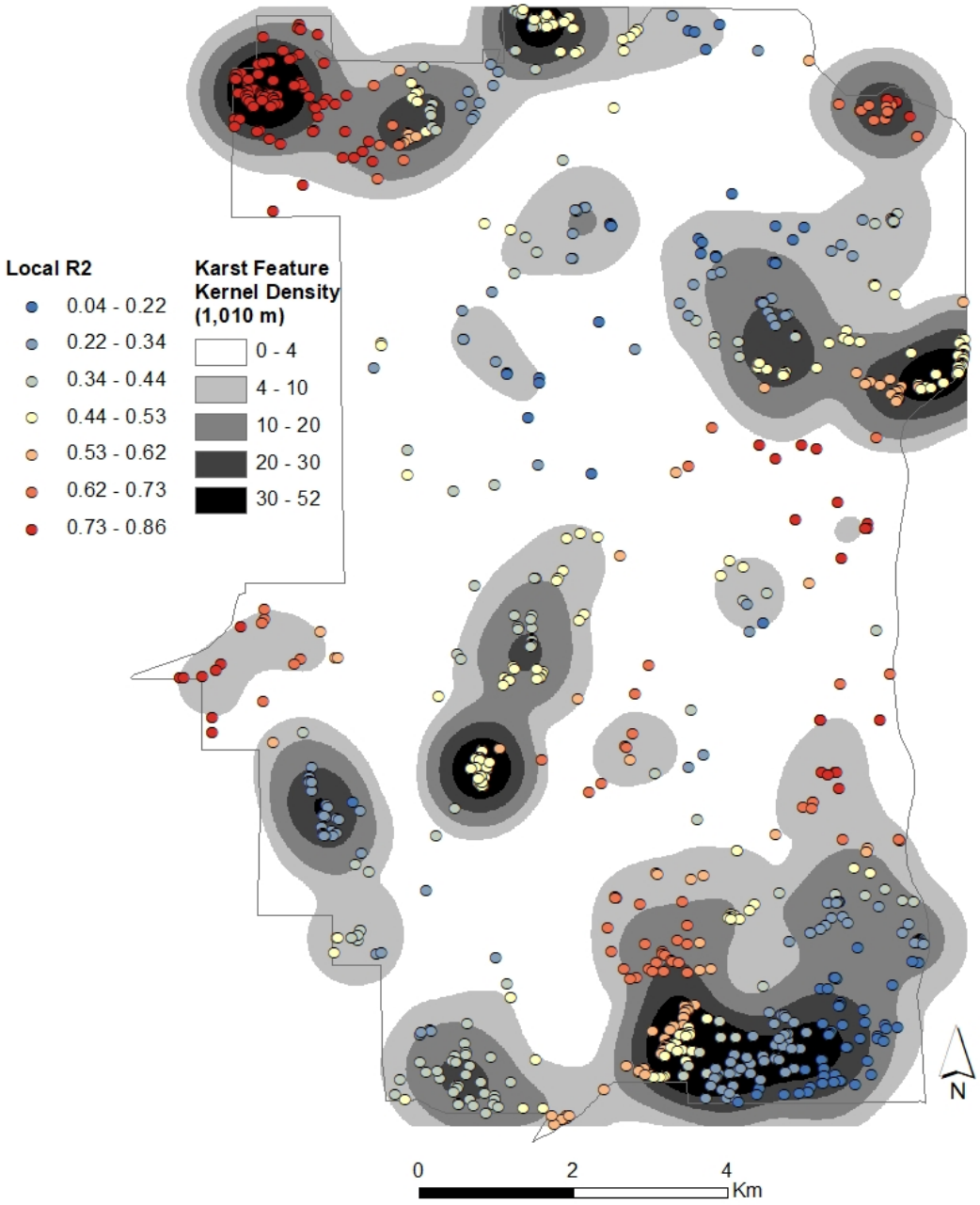

Figure 12. GWR local R^2 map. Values are mapped above KFKD.

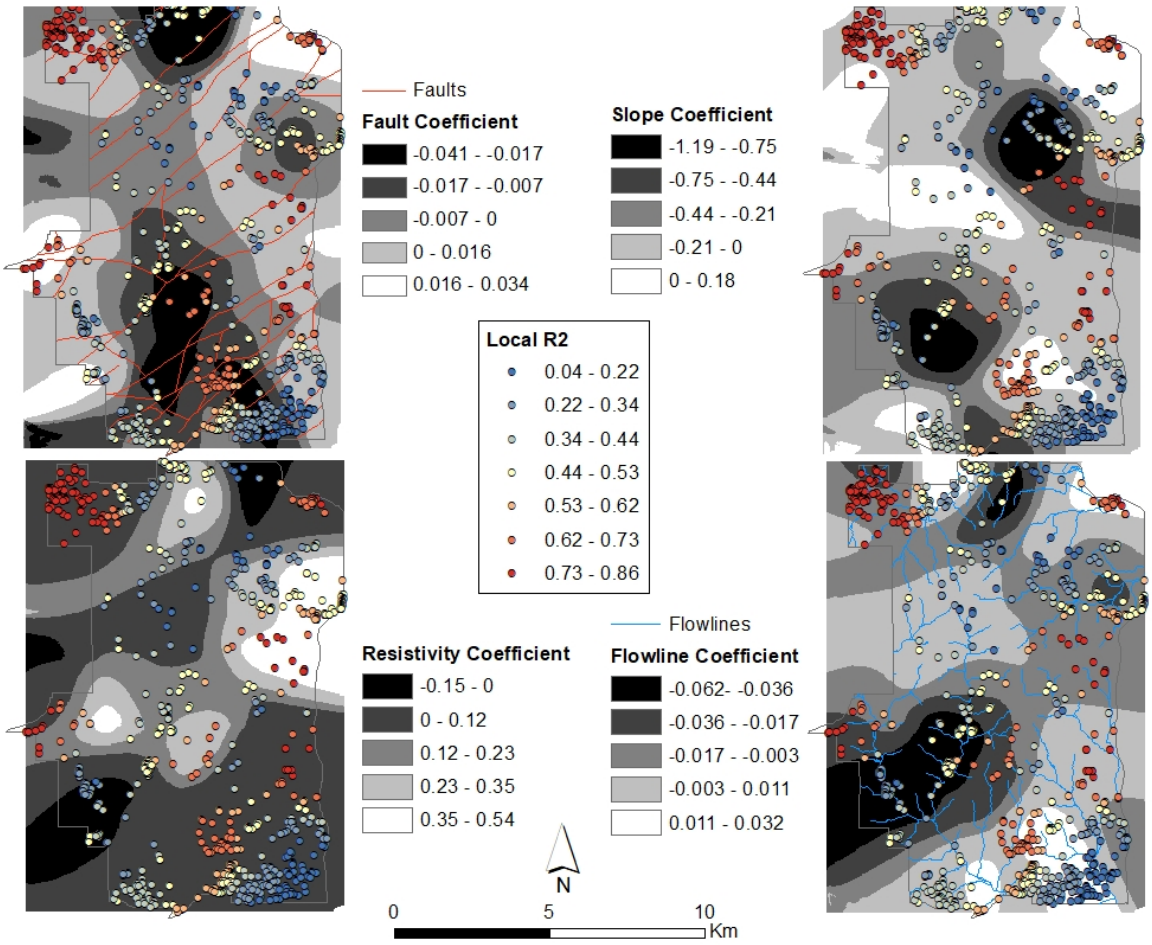

Figure 13. Local coefficient estimates of GWR model

Where coefficient estimates for distance from flowlines and faults (Figure 13) are negative, it indicates that areas with high KFKD can be found hear faults and flowlines. In areas where slope coefficient is negative (grays and black), areas with high KFKD were found near flatter slopes, and vice versa (Figure 13). For resistivity, areas with positive coefficients indicate that KFKD and resistivity are directly correlated.

IV. DISCUSSION

Camp Bullis data were not available at the start of this project and therefore not available to help guide the Freeman Center karst survey design. Ideally, with prior access to this full-coverage data set, sampling strategies and designs could have been experimentally tested prior to data collection in the field. Unfortunately, this was not the case during this study, and the Camp Bullis data were only available for a retrospective analysis. The ideal case was to create a predicted karst feature kernel density map for Freeman so that future research would have areas to focus survey efforts on. However, GWR results from Bullis are not applicable to Freeman because GWR is a local model and predictions are applicable only within the study area. I also considered applying the global OLS model to Freeman but decided against it because the model performance was minimal (R^2= 0.30) due to missing explanatory variables and the high non-stationarity of the explanatory variables. Another factor that could affect model performance is the locations of the high KFKD clusters being near the edges of the Bullis boundary. Coefficient estimates and model performance near edges could be spurious.

The model misspecification deserves more study. In the Doctor and Doctor (2012) and Doctor et al. (2008) sinkhole occurrence studies, the GWR models performed well with only proximity variables (proximity to nearest factor) and both of the study areas exhibit extensive structural features like fold axes and fracture traces. However, for the Camp Bullis models, proximity factors have smaller coefficients than slope and resistivity, which could indicate that geomorphology and geologic materials influence karst feature occurrence more than structural factors like faults in this area. As previously mentioned, most spatial studies focus on large and easily-detected sinkholes for hazard

mapping and sinkhole potential studies. These features are larger and therefore might be more affected by regional processes like structure, geologic materials, and hydrological factors. Poor performance and misspecification of the models for karst feature density could be the result of complex factors affecting smaller scale karst features, suggesting that modeling this process could be difficult.

For future karst feature surveys on the Freeman Center, or in other areas of the Edwards Recharge Zone, we suggest testing additional methods, such as surveying transects instead of distributed plots. In addition to requiring less effort logistically, this method covers more distance and more diverse terrain characteristics, therefore increasing possibility of finding karst features.

Of the 37 total subsidence sinkholes recorded during surveying, none were reflected in the resulting 414 sinks from the procedure because the area cutoff was $16m^2$ and the average diameter for the subsidence sinkholes was approximately 1 meter. In order to find smaller scale, subsidence sinkholes higher horizontal accuracy LiDAR data should be used with the Filled-Sink Difference procedure. This would ultimately increase total sinks found, both false and true sinkholes. To remove false sinkholes, diagnostic morphometric parameters for sinkholes within the Edwards Aquifer Recharge Zone such as depth, diameter, and circularity should be identified and used as criteria for selection in future studies to improve the detection of true sinkhole diversity, therefore increasing the possibility of finding smaller scale karst features.

It bears mentioning that an exploratory study on karst feature distribution of this kind should not be misinterpreted as providing estimates of probability of karst feature or sinkhole formation because risk assessments require study of development through time

(Doctor and Doctor, 2012). The results of this exploratory study are not meant to provide a replacement for visual inspection and field verification that are required by TCEQ rules. However, further investigation of the factors influencing karst feature presence could be helpful in developing land conservation and acquisition decision models.

V. CONCLUSION

This study tested a statistically-designed partial karst feature inventory method using geologic and other spatial data to determine that, with this particular method, a representative karst feature density could not be estimated with a partial survey. The primary reason is because karst features tend to cluster, which precludes accurate results using random survey points. Although more time and resource-intensive, full coverage surveys ensure proper characterization of an area's karst feature density and sensitivity. Variables significant in explaining karst feature density in a full-coverage model were slope, apparent resistivity, distance to nearest flowline, and location within Edwards Aquifer hydrostratigraphical units. These controlling factors, however, still resulted in models that exhibit spatial autocorrelation in residuals and were misspecified; indicating a missing explanatory variable. Despite this, these methods provided a better understanding of factors controlling karst feature density and can be used as a starting point in future research.

REFERENCES

Barker, R.A., Bush, P.W., and Baker, E.T.J., 1994, Geologic history and hydrogeologic setting of the Edwards-Trinity aquifer system, west-central Texas: Water Resources Investigations 94-4039 http://pubs.er.usgs.gov/publication/wri944039.

Blome, C.D., Faith, J.R., Pedraza, D.E., Ozuna, G.B., Cole, J.C., Clark, A.K., Small, T.A., and Morris, R.R., 2005, Geologic map of the Edwards aquifer recharge zone, southcentral Texas: U.S. Geological Survey Scientific Investigations Map 2873, scale 1:200,000.

Brinkmann, R., Parise, M., and Dye, D., 2008, Sinkhole distribution in a rapidly developing urban environment: Hillsborough County, Tampa Bay area, Florida: Engineering Geology, v. 99, p. 169–184, doi: 10.1016/j.enggeo.2007.11.020.

Capital Area Council of Governments (CAPCOG). Capital Area Council of Governments Lidar, 2012-01-01. Web. 2018-02-22.

Carter, J., Schmid, K., Waters, K., Betzhold, L., Hadley, B., Mataosky, R., Halleran, J., and NOAA Coastal Services Center, 2012, Lidar 101 : An Introduction to Lidar Technology , Data , and Applications:, doi: 10.5194/isprsarchives-XL-7-W3-1257-2015.

Clark, A.K., 2003, Geologic Framework and Hydrogeologic Features of the Glen Rose Limestone, Camp Bullis Training Site, Bexar County, Texas: Water-Resources Investigations Report 03–4081.

Doctor, D.H., and Doctor, K.Z., 2012, Spatial analysis of geologic and hydrologic features relating to sinkhole occurrence in Jefferson County, West Virginia: Carbonates and Evaporites, v. 27, p. 143–152, doi: 10.1007/s13146-012-0098-1.

Clark, A.K., Golab, J.A., and Morris, R.R., 2016, Geologic framework and hydrostratigraphy of the Edwards and Trinity aquifers within northern Bexar and Comal Counties, Texas: U.S. Geological Survey Scientific Investigations Map 3366, 1 sheet, scale 1:24,000, pamphlet, https://doi.org/10.3133/sim3366

Doctor, D.H., and Young, J.A., 2013, An evaluation of Automated Gis Tools for Delineating Karst Sinkholes and Closed Depressions From 1-Meter Lidar-Derived Digital Elevation Data: Thirteenth Multidisciplinary Conference on Sinkholes and the Engineering and Environmental Impacts of Karst, p. 449–458, doi: PNR61.

EAA Edwards Aquifer Authority: The EAA Act: A Success Story, https://www.edwardsaquifer.org/.

Esri, 2017, Collector for ArcGIS, version 18.0.3, build 1033

Florea, L.J., Paylor, R.L., Simpson, L., and Gulley, J., 2002, Karst GIS advances in Kentucky: Journal of Cave and Karst Studies, v. 64, p. 58–62.

Fotheringham, A.S., Brunsdon, C., and Charlton, M., 2002, Geographically weighted regression: the analysis of spatially varying relationships: Wiley.

Gao, Y., Alexander, E.C., and Barnes, R.J., 2005, Karst database implementation in Minnesota: Analysis of sinkhole distribution: Environmental Geology, v. 47, p. 1083–1098, doi: 10.1007/s00254-005-1241-2.

Gary, M.O., Rucker, D.F., Smith, B.D., Smith, D. V, and Befus, K., 2013, Geophysical Investigations of the Edwards-Trinity Aquifer System at Multiple Scales: Interpreting Airborne and Direct-Current Resistivity in Karst: *in* 13th Sinkhole Conference- National Cave and Karst Research Institute, p. 195-206. 10.5038/9780979542275.1127.

Gutiérrez, F., Parise, M., De Waele, J., and Jourde, H., 2014, A review on natural and human-induced geohazards and impacts in karst: Earth-Science Reviews, v. 138, p. 61–88, doi: 10.1016/j.earscirev.2014.08.002.

Hauwert, N., Johns, D., Hunt, B., Beery, J., Smith, B., and Sharp, J.M.J., 2004, Flow systems of the Edwards Aquifer Barton Springs Segment Interpreted from Tracing and Associated Field Studies, *in* Edwards Symposium, p. 1–18, http://www.bseacd.org/uploads/Hauwert et al_, 2004, Edwards Symposium.pdf.

Hunt, B.B., Smith, B.A., Andrews, A., Wierman, D.A., Broun, A.S., and Gary, M.O., 2015, Relay Ramp Structures and Their Influence on Groundwater Flow in the Edwards and Trinity Aquifers, Hays and Travis Counties, Central Texas, *in* Sinkholes and the Engineering and Environmental Impacts of Karst: Proceedings of the Fourteenth Multidisciplinary Conference, p. 189–200, doi: 10.5038/9780991000951.1081.

Johnson, S., Schindel, G., Veni, G., Hauwert, N., Hunt, B., Smith, B., and Gary, M., 2012, Tracing groundwater Flowpaths in the Vicinity of San Marcos springs, Texas:, http://www.edwardsaquifer.org.

Kobal, M., Bertoncelj, I., Pirotti, F., and Kutnar, L., 2014, Lidar processing for defining sinkhole characteristics under dense forest cover: A case study in the dinaric mountains, *in* ISPRS Technical Commission VII Symposium, The International Archives of the Photogrammetry, Remote Sensing and Spatial Information Sciences, v. XL–7, p. 113–118, doi: 10.5194/isprsarchives-XL-7-113-2014.

Lindsey, B.D., Katz, B.G., Berndt, M.P., Ardis, A.F., and Skach, K.A., 2010, Relations between sinkhole density and anthropogenic contaminants in selected carbonate aquifers in the eastern United States: Environmental Earth Sciences, v. 60, p. 1073–1090, doi: 10.1007/s12665-009-0252-9.

Maidment, D.R. (Ed.), 2002, Arc Hydro: GIS for Water Resources: Esri Press.

Panno, S. V., and Luman, D.E., 2018, Characterization of cover-collapse sinkhole morphology on a groundwater basin-wide scale using lidar elevation data: A new conceptual model for sinkhole evolution: Geomorphology, v. 318, p. 1–17, doi: 10.1016/j.geomorph.2018.05.013.

RStudio, 2017, R version 3.4.3 URL http://www.rstudio.com/

Sharp, J.M., and Banner, J.L., 1997, The Edwards aquifer: A resource in conflict: GSA Today, v. 7, p. 1–9.

Slade, R.M., Dorsey, M.E., and Stewart, S.L., 1986, Hydrology and water quality of the Edwards Aquifer associated with Barton Springs in the Austin area, Texas: U.S. Geological Survey Water-Resources Investigations Report, p. 117, http://www.karstportal.org/sites/karstportal.org/files/KIP-00011534.pdf.

Smith, B.B.D., Cain, M.J., Clark, A.K., Moore, D.W., Faith, J.R., and Hill, P.L. Helicopter Electromagnetic and Magnetic Survey Data and Maps , Northern Bexar County , Texas

Stein, W.G., and Ozuna, G.B., 1994, Geologic framework and hydrogeologic characteristics of the Edwards aquifer outcrop, Comal County, Texas: USGS Water-Resources Investigations Report 94-4117

Texas Commission on Environmental Quality, 2004, Instructions to Geologists for Geologic Assessments on the Edwards Aquifer Recharge/Transition Zones.

Texas Commission on Environmental Quality, 2008a, Chapter 213 Subchapter A: Edwards Aquifer in Medina, Bexar, Comal, Kinney, Uvalde, Hays, Travis, and Williamson Counties; Texas Administrative Code

Texas Commission on Environmental Quality, 2008b, Chapter 213 Subchapter B: Contributing Zone to the Edwards Aquifer in Medina, Bexar, Comal, Kinney, Uvalde, Hays, Travis, And Williamson Counties; Texas Administrative Code

Texas Natural Resources Information System (TNRIS), Texas Rivers, Streams, and Waterbodies, 2014-02-01. Web. 2019-07-04.

TNRIS, Texas TOP Imagery, 2015-12-31. Web. 2019-07-04.

TWDB, 2017, Texas Water Development Board 2017 State Water Plan - State Population and Water Supplies.

U.S. Department of Agriculture, Natural Resources Conservation Service, 2017, Soil Survey Geographic (SSURGO) database for Comal and Hays Counties, Texas; tx604; https://websoilsurvey.sc.egov.usda.gov/

U.S. Department of Agriculture, Soil Conservation Service, 1984, Soil Survey of Comal and Hays Counties Texas.

Veni, G., 1994, Geomorphology, hydrogeology, geochemistry, and evolution of the karstic Lower Glen Rose aquifer, south-central Texas: Pennsylvania State University, dissertation, doi: 10.16953/deusbed.74839.

Wall, J., Bohnenstiehl, D.R., Wegmann, K.W., and Levine, N.S., 2017, Morphometric comparisons between automated and manual karst depression inventories in Apalachicola National Forest, Florida, and Mammoth Cave National Park, Kentucky, USA: Natural Hazards, v. 85, p. 729–749, doi: 10.1007/s11069-016-2600-x.

Wu, Q., Deng, C., and Chen, Z., 2016, Automated delineation of karst sinkholes from LiDAR-derived digital elevation models: Geomorphology, v. 266, p. 1–10, doi: 10.1016/J.GEOMORPH.2016.05.006.

Zhu, J., and Pierskalla, W.P.J., 2016, Applying a weighted random forests method to extract karst sinkholes from LiDAR data: Journal of Hydrology, v. 533, p. 343–352, doi: 10.1016/j.jhydrol.2015.12.012.

Zhu, J., Taylor, T.P., Currens, J.C., and Crawford, M.M., 2014, Improved karst sinkhole mapping in Kentucky using LiDAR techniques: A pilot study in Floyds fork watershed: Journal of Cave and Karst Studies, v. 76, p. 207–216, doi: 10.4311/2013ES0135.